Appl Magn Reson (2010) 37:505–514
DOI 10.1007/s00723-009-0069-4

Applied
Magnetic Resonance

EPR Characterization of a Rigid Bis-TEMPO–Bis-Ketal for Dynamic Nuclear Polarization

Marat Gafurov · Sevdalina Lyubenova · Vasyl Denysenkov · Olivier Ouari · Hakim Karoui · François Le Moigne · Paul Tordo · Thomas Prisner

Received: 11 May 2009 / Revised: 2 June 2009 / Published online: 11 November 2009

Abstract We have characterized the rigid binitroxide radical bis-TEMPO–bis-Ketal (bTbK) by continuous-wave (CW) and pulsed electron paramagnetic resonance (EPR) spectroscopy performed at X-band (9 GHz) and G-band (180 GHz) frequencies. bTbK has been successfully used for dynamic nuclear polarization (DNP)-enhanced solid-state nuclear magnetic resonance (SS-DNP) experiments based on the cross-effect, which involves two electrons and one nuclear spin, and gave very high signal enhancements. For a quantitative description of the polarization enhancements and their excitation frequency profile, a detailed information about the values and relative orientation of the magnetic hyperfine-, dipolar-, **g**-tensors and the exchange interaction of the two unpaired electron spins within the molecule is mandatory. We have determined these tensors and their relative orientation by CW-EPR spectra and pulsed electron double resonance experiments in frozen solution. The potential of using the cross-effect also for DNP in liquid solutions has been experimentally investigated by room-temperature high-field DNP experiments performed at 9.2 T.

1 Introduction

Recently, dynamic nuclear polarization (DNP) is of increased interest regarding applications in structural biology, material science and analytical chemistry [1]. Especially the possibility to obtain large enhancements of the nuclear spin polarization in solids at magnetic fields larger than 5 T triggered many new

M. Gafurov · S. Lyubenova · V. Denysenkov · T. Prisner (✉)
Institute of Physical and Theoretical Chemistry, Center of Biomolecular Magnetic Resonance, Goethe University, Max-von-Laue Str.7, 60438 Frankfurt am Main, Germany
e-mail: prisner@chemie.uni-frankfurt.de

O. Ouari · H. Karoui · F. Le Moigne · P. Tordo
Provence Chemistry Laboratory, UMR 6264, Provence University, CNRS, 13397 Marseilles Cedex 20, France

scientific initiatives in this field. One important result gathered by the group of R. Griffin was that the cross-effect [2] can be superior to the solid-effect [3] at high magnetic field strengths (see Ref. [4] for a review). The cross-effect describes the coupling between two close-by electron spins, coupled to a nuclear spin. Biradicals have been used to yield polarization enhancements up to 150 at magnetic fields of 5 T and temperatures of 100 K [5]. The obtainable enhancement depends on the electron spin–spin coupling, the difference in their respective Larmor frequencies, relaxation properties and line widths, as well as the interactions with neighboring nuclear spins. It has been demonstrated that the transfer of polarization to the coupled nuclear spins is optimized if the difference in the Larmor frequencies of the two electron spins matches the nuclear spin Larmor splitting:

$$\omega_{e1} - \omega_{e2} \approx \pm \omega_I \tag{1}$$

and if the dipolar coupling between the two electron spins is large.

Nitroxide radicals are often used as DNP polarizing agents in biological samples. For these radicals the electron spin Larmor frequency is dominated by the anisotropic **g**-tensor and, therefore, is strongly orientation dependent. It has been shown that the mutual orientation of the two nitroxides in such biradicals drastically effects the maximum obtainable enhancements [6]. Therefore, a detailed electron paramagnetic resonance (EPR) study of such biradicals is important for the understanding and optimization of the DNP effect. Here, we describe the EPR characterization of the nitroxide biradical bis-TEMPO–bis-Ketal (bTbK), which exhibits a rigid geometry.

EPR can be used to characterize many of the spin interactions of mono- and poly-nitroxide radicals important for the DNP cross-effect [6–8].

The full spin Hamiltonian for the nitroxide biradicals (two spins with $S = 1/2$ and $I = 1$ for ^{14}N) is commonly expressed as

$$\hat{H} = \hat{H}^{Z}_{1S} + \hat{H}^{Z}_{2S} + \hat{H}^{HF}_{1SI} + \hat{H}^{HF}_{2SI} + \hat{H}^{DD}_{SS} + \hat{H}^{J}_{SS} + \hat{H}^{Z}_{1I} + \hat{H}^{Z}_{2I}. \tag{2}$$

$\hat{H}^{Z}_{1S}$ and $\hat{H}^{Z}_{2S}$ reflect the Zeeman interactions of electron spins 1 and 2, respectively, with the external magnetic field **B** dominated by the anisotropic **g**-tensors. $\hat{H}^{Z}_{1I}$ and $\hat{H}^{Z}_{2I}$ are the Zeeman interactions of the nuclear spins 1 and 2, respectively.

In the high-field approach, the electron Zeeman interaction in the eigenframe of the $\mathbf{g_1}$ tensor (where it has only the diagonal components g_{xx}, g_{zz} and g_{yy}) is

$$\hat{H}^{Z}_{1S} = \beta(\mathbf{B}g_1S_1) = \left(g^2_{1xx}l^2_x + g^2_{1yy}l^2_y + g^2_{zz}l^2_z\right)^{1/2}\beta\mathbf{B}S_{1z}$$
$$\text{(and similar for the second spin and nuclear Zeeman interactions)}, \tag{3}$$

where β is the Bohr magneton and l_x, l_y and l_z are the direction cosines relative to the applied field direction. The axis system in which our results are described is shown in Fig. 1. The direction of x_1-axis is along the N–O bond, while z_1 is perpendicular to the plane of the 2,2,6,6-tetramethyl-1-piperidine-1-oxy (TEMPO) ring system. Direction of y_1 is chosen to form a right-handed Cartesian coordinate system.

The transformation from the principal axis system of $\mathbf{g_2}$ to that of $\mathbf{g_1}$ is described by the three Euler angles: α, β and γ. To simulate a solid-state spectrum, the integration over all possible values of another set of two Euler angles (φ and θ), defining the mutual orientation of the molecular and laboratory systems, should be performed.

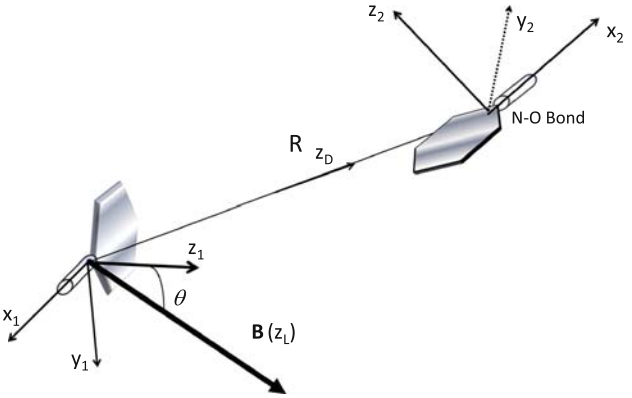

Fig. 1 Molecular (hyperfine and **g**-tensor) and dipolar axis systems for the bTbK biradical, as defined in the text

$\hat{H}_{1SI}^{\mathrm{HF}}$ and $\hat{H}_{2SI}^{\mathrm{HF}}$ are the hyperfine (HF) interactions between each electron and nucleus (^{14}N), inside the monoradical moieties 1 and 2, respectively, described in the hyperfine main axis system by the anisotropic hyperfine tensor **A**:

$$\hat{H}_{1SI}^{\mathrm{HF}} = A_{1xx}S_{1x}I_{1x} + A_{1yy}S_{1y}I_{1y} + A_{1xx}S_{1z}I_{1z}. \quad (4)$$

The main axes of the hyperfine tensor **A** and of the anisotropic **g**-tensor are taken to be collinear, the values of their corresponding components for spin 1 and 2 due to the symmetry of the system are taken to be identical, i.e., $g_{1ii} = g_{2ii} = g_{ii}$, $A_{1ii} = A_{2ii} = A_{ii}$, where $i = \{x, y, z\}$.

$\hat{H}_{SS}^{DD}$ and $\hat{H}_{SS}^{J}$ are the dipole–dipole (anisotropic) and exchange (isotropic) interactions between the two electron spins, described by the isotropic exchange coupling J and the anisotropic dipolar interaction tensor **D**. The dipole–dipole interaction in its main axes, with z_D aligned along the vector **R** connecting the electron spins, is expressed as

$$\hat{H}_{SS}^{DD} = D_{xx}S_{1x}S_{2x} + D_{yy}S_{1y}S_{2y} + D_{zz}S_{1z}S_{2z} = D\left(S_{1z}S_{2z} - \frac{1}{2}S_{1x}S_{2x} - \frac{1}{2}S_{1y}S_{2y}\right), \quad (5)$$

assuming axial symmetry, $D_{xx} = D_{yy}$. The transformation of the dipole–dipole coordinate system to the molecular frame is determined by two additional Euler angles, η and ξ. This interaction can be detected only in solutions with a high viscosity, in oriented structures, or in frozen solutions. Sufficiently rapid rotation of the molecules of the mono- and biradicals leads to complete averaging of the dipole–dipole interaction (together with the anisotropic Zeeman and HF interactions). Thus, in the EPR spectra of solutions with a sufficiently low viscosity, it is possible to detect only the isotropic exchange interaction $\hat{H}_{SS}^{J} = JS_1S_2$.

2 Materials and Methods

Bis-TEMPO–bis-Ketal was synthesized in a two-step sequence with 26% overall yield following the reaction scheme as previously described [9]. The bispiroketal skeleton was obtained by reacting pentaerythritol (0.87 g, 6.4 mmol) with 2,2,6,6-

tetramethyl-4-piperidone (2.00 g, 12.8 mmol) in the presence of *p*-toluenesulfonic acid (2.21 g, 12.8 mmol) in toluene at reflux. bTbK was obtained as orange crystals by oxidation of the corresponding diamine at 0°C with 1.5 equivalents of meta-chloroperoxybenzoic acid in CH_2Cl_2. The average distance R between N–N and O–O calculated from the bTbk crystal structure is 1.18 nm.

EPR measurements were performed on X- (9 GHz, Bruker) and G-band (180 GHz, home-built) spectrometers in Frankfurt at room (RT) and low (40–90 K, LT) temperatures using both continuous-wave (CW) and pulsed methods.

X-band CW-EPR spectroscopy. The X-band CW-EPR spectra were recorded on a Bruker Elexsys-500 X-band spectrometer using a standard rectangular Bruker EPR cavity (ER4102T) equipped with an Oxford helium cryostat (ESR900). The microwave (mw) frequency was measured using a Systron Donner frequency counter (6054D), and the magnetic field was measured using a Bruker gaussmeter (ER035M).

X-band pulse-EPR spectroscopy. Pulsed electron double resonance measurements were performed on a Bruker Elexsys-580 X-band spectrometer equipped with a Bruker MD5-W1 cavity and an Oxford CF935 helium flow cryostat with an ITC-5025 temperature controller. The second microwave frequency was coupled into the microwave bridge by a commercially available setup (E580-400U) from Bruker. The four-pulse pulsed electron double resonance (PELDOR) experiments were carried out using the pulse sequence $t_p(\pi/2)_{det} - \tau_1 - t_p(\pi)_{det} - (\tau_2 + t) - t_p(\pi)_{pump} - (\tau_2 + t) - t_p(\pi)_{det} - \tau_2 -$ echo. The pump frequency $\nu(\mathrm{mw})_{pump}$ was set to the center of the bTbK EPR spectrum, while the detection frequency $\nu(\mathrm{mw})_{det}$ had an offset of −80 MHz.

G-band CW-EPR spectroscopy. 180 GHz home-built spectrometer (see Ref. [10] for details) controlled by Specman4EPR software program [11] was used. EPR of ^{55}Mn in powdered MgO with the known parameters [$A = 8.710(3)$ mT and $g = 2.00101(5)$] was exploited as an internal reference [12, 13] in order to calibrate the magnetic field to define the values of **g**-, **A**- and **D**-tensors.

In situ DNP measurements at room temperatures in a field of 9.2 T (260 GHz microwave frequency and 400 MHz radio frequency) using a double-resonance structure were carried out on a homebuilt Frankfurt liquid-state DNP-spectrometer (see Ref. [14] for details).

The samples consisted of 120 µl 100 µM bTbK in d_8-toluene for X-band and 0.25 µl of 2 mM bTbK in d_8-toluene for G-band EPR experiments. DNP measurements were performed on samples of 4 nl of 10 mM bis-nitroxide in dichloromethane.

Simulation and fitting. X- and G-band EPR spectra were calculated with the EasySpin package [15] and a home-written program as described in one of the previous publications [16] was used for the PELDOR simulations.

3 Results

3.1 RT CW X-Band Spectrum

A CW X-band EPR spectrum of the bTbK at RT was recorded to investigate potential exchange coupling between the two nitroxide radicals in the molecule. The

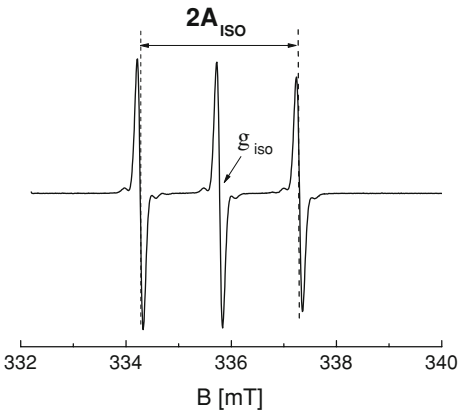

Fig. 2 RT X-band spectrum of 125 μM bTbK in d_8-toluene. $\nu_{mw} = 9.63$ GHz, $B_{mod} = 0.3$ G at 100 kHz

experimental results obtained in d_8-toluene are shown in Fig. 2. The spectrum is very similar to that of a monoradical and exhibits three hyperfine lines with an isotropic hyperfine splitting, $A_{iso} = 15.1(2)$ G, centered at the isotropic g-value $g_{iso} = 2.0063(2)$, with a hyperfine line width of $\Delta H_{PP} \approx 1.2$ G.

3.2 RT CW G-band Spectrum

The liquid G-band spectrum shows broader lines with $\Delta H_{PP} \approx 7.2$ G (Fig. 3), which can be attributed to the rotational motion of the molecule (see Sect. 4). We did not observe any line broadening due to intermolecular interactions for concentrations ranging from 0.2 to 4 mM.

3.3 LT CW X-Band Spectra

X-band CW-EPR spectra of TEMPO and bTbK in frozen solution of toluene are shown in Fig. 4. From these spectra the hyperfine coupling $A_{zz} \approx 33.7(5)$ G could be determined. Additionally, a dipolar splitting of 7.9 G (22.1 MHz) could be observed on the hyperfine lines.

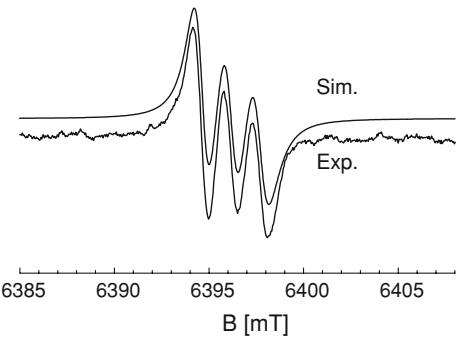

Fig. 3 RT G-band spectrum of 2 mM bTbK in d_8-toluene ($\nu_{mw} = 179.8$ GHz, $B_{mod} = 1$ G at 20 kHz) together with a simulation based on the fitting parameters given in Table 1 and a rotational correlation time $\tau_c = 55(15)$ ns

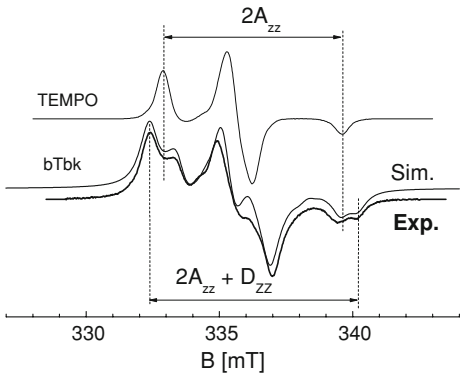

Fig. 4 LT X-band EPR spectrum of frozen solution of 125 μM bTbK (*bottom*) at $T = 70$ K ($\nu_{mw} = 9.63$ GHz, $B_{mod} = 0.3$ G at 100 kHz) together with the spectrum simulated using the parameters given in Table 1. An EPR spectrum of the monoradical TEMPO taken under the same experimental conditions is shown for a comparison

3.4 LT CW G-Band Spectra

High-field EPR at $\approx$180 GHz in frozen solution (Fig. 5) allows the determination of the values of **g**-tensor. The value of g_{xx} for the bTbK is larger compared to TEMPO.

Accurate determination of g_{xx} from the spectrum in this case is not straightforward (cf. Refs. [17, 18]; Fig. 5), calculations result in a value of $g_{xx} \approx 2.0105(5)$ (see Table 1).

The hyperfine component $A_{zz} = 35(1)$ G [=98(3) MHz] resolved in the high-field region of CW-EPR spectrum is in good agreement with the X-band measurements. Moreover, a dipolar splitting of 7.25 G (20.3 MHz) could be resolved at the g_{zz} spectral position and 9.5(5) G [=27(1) MHz] for the central line (g_{yy}).

3.5 LT Pulsed X-Band PELDOR

Figure 6 shows four-pulse PELDOR measurement (for details of the experiment see the figure caption) performed at 9 GHz. Clear dipolar oscillations with the frequency of 29.5 MHz could be observed only in the case of short detection and

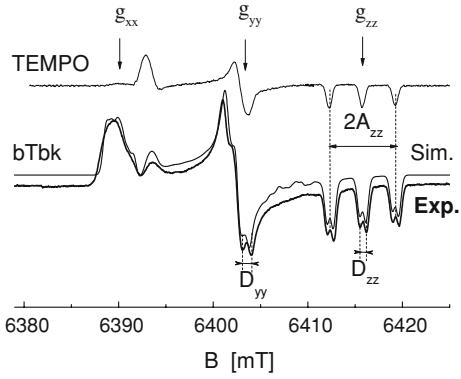

Fig. 5 LT G-band spectrum at $T = 70$ K ($\nu_{mw} = 179.8$ GHz, $B_{mod} = 0.5$ G at 20 kHz) of 2 mM bTbK in frozen solution together with the spectrum simulated using the parameters given in Table 1. For comparison, the spectrum of 2 mM TEMPO taken under identical experimental conditions is shown

Table 1 EPR parameters of the biradcial bTbK obtained from the X- and G-band experiments

g_{xx}	2.0105(5)	A_{xx}	6(1) G	J	≈ 0
g_{yy}	2.0065(1)	A_{yy}	5(1) G	D	10.8(3) G [R = 12.0(1) Å]
g_{zz}	2.0024(1)	A_{zz}	34(1) G	α	−58(5)
				β	79(10)
				γ	−118(5)
g_{iso}	2.0064(3)	A_{iso}	15(1) G	(η, ξ, 0)	(0(10), 65(10),0)

Lorentzian line widths of 4.2 and 6.0 G were used for the fit of the solid-state 9 and 180 GHz spectra, respectively. The distance R is derived from the line splitting, using D [G] $\approx$ 18560/r^3 [Å]. Euler angles (α, β, γ) and (η, ξ) of the rotational transformation of the $\mathbf{g_2}$- and **D**-principal axis systems to that of $\mathbf{g_1}$, correspondingly, are given in *zyz* convention in degrees

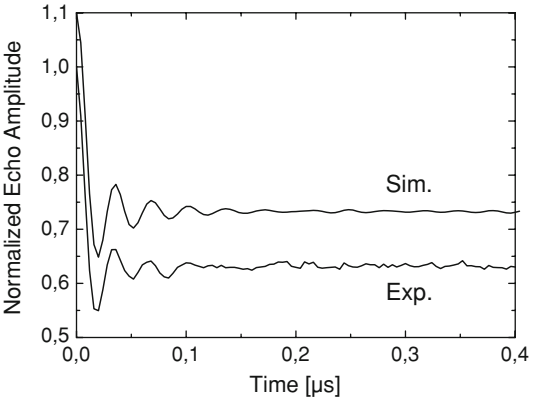

Fig. 6 X-band PELDOR time trace of 100 µM bTbK in d_8-toluene. Experimental conditions: $T = 40$ K, $\nu(\mathrm{mw})_{\mathrm{pump}} = 9.69$ GHz, $\nu(\mathrm{mw})_{\mathrm{detection}} = 9.61$ GHz, $t_p(\pi)_{\mathrm{pump}} = 12$ ns, $t_p(\pi/2)_{\mathrm{det}} = t_p(\pi) = 12$ ns, $\tau_1 = 452$ ns $\tau_2 = 1000$ ns, repetition rate, 0.25 kHz, scans accumulated, 250, number of points, 200, $\Delta t = 4$ ns. The normalized simulation with the proposed geometry of the biradical and with a distance of $R = 1.18$ nm and a distance distribution of $\Delta R = 0.05$ nm is shown above the normalized experimental trace (offset by 0.1)

pump pulses. This can be explained by the short distance of the two unpaired electron spins resulting in a strong dipolar coupling between them.

Simulations of the PELDOR time traces reveal an electron–electron distance of 1.18 nm with the distance distribution of 0.05 nm, which is in agreement with the average distance calculated from the crystal structure [9].

3.6 RT DNP at 260 GHz/400 MHz

Because of the restricted solubility of bTbK in water, numerous organic solvents (dimethyl sulfoxide, ethanol, benzene, toluene and dichloromethane) were investigated for the DNP measurements. An enhancement between −2 and −3 was achieved on the protons of dichloromethane at spin concentration of 10 mM, when the microwave frequency was resonant with the central hyperfine transition (Fig. 7). This value is very similar to the DNP enhancement obtained with the monoradical TEMPO under the same conditions.

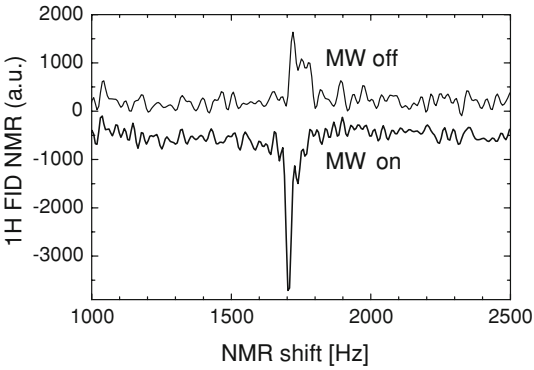

Fig. 7 RT nuclear magnetic resonance (NMR) spectrum of the free induction decay (FID) from the ^{1}H nuclei of dichlormethane (CH_2Cl_2), containing 5 mM of bTbK (10 mM of unpaired electron spins). $\nu_{rf} = 392$ MHz, $\nu_{mw} = 258.6$ GHz. (*Upper trace*) without mw excitation, (*lower trace*) with 25 mW continuous mw irradiation

4 Discussion

Both, X- and G-band EPR solid spectra, reveal a dipolar splitting. At X-band frequencies the A_{zz} component is spectrally well resolved (Fig. 4) and the dipolar splitting was observed most clearly on the outer hyperfine lines. At G-band frequencies the dipolar splitting is seen on all three hyperfine lines at the g_{zz} position as well as on the g_{yy} position. At the g_{xx} position only a broad unresolved peak can be observed, but the G-band experiments show that the g-value at this position is markedly larger compared to a TEMPO nitroxide radical (Fig. 5). Due to the strong anisotropy of the **g**-tensor, the difference between the electron spin Larmor frequencies for orientations $\mathbf{y} \parallel \mathbf{B}$ and $\mathbf{z} \parallel \mathbf{B}$ can match the proton Larmor frequency in solid-state (SS) phase (see Eq. (1); Fig. 5), facilitating cross-effect driven SS-DNP.

Both solid spectra at X- and G-band frequencies could be simulated satisfactorily with a set of tensor orientations and couplings given in Table 1. The obtained values are in good agreement with the geometry from the X-ray structure (Fig. 8), where the directions of the two N–O bonds are almost parallel and the two out-of-plane vectors **z** of the nitroxide moieties are perpendicular to each other and to the spin–spin connecting vector **R**.

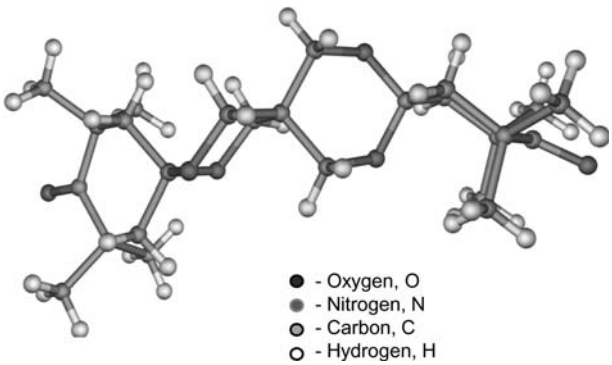

Fig. 8 Molecular structure of the bTbK biradical, as obtained from X-ray single crystal data

The RT X-band EPR spectra (Fig. 2) prove that the exchange coupling J is negligible compared to the dipolar coupling between the two nitroxide moieties, despite the short distance between the two radical centers. Simulation of the X-band PELDOR time traces (Fig. 6) further supports this geometry and the distance between the two unpaired spins. Therefore, bTbK possesses an optimized geometry for solid-state DNP at high magnetic fields, mediated by the cross-effect. Indeed, SS-DNP experiments performed at 5 T showed the largest enhancements observed so far for biradicals [9].

The situation concerning DNP in liquid solutions differs. Because of the rotational motion, the liquid spectrum at 260 GHz is motional narrowed. The motional narrowed 180 GHz CW-EPR spectra (Fig. 3) could be simulated by a rotational correlation time of $\tau_c = 55(15)$ ns and is therefore spectrally much narrower compared to the proton Larmor frequency of 400 MHz. Therefore, matching of the difference in resonance frequencies of the two unpaired electron spins with the proton Larmor frequencies cannot be fulfilled in liquid solutions. Thus, it was not surprising that the observed DNP enhancements achieved with the biradcial in liquid solutions are purely caused by the classical Overhauser effect [19] and not by cross-effects, involving two electron spins.

An immobilized biradical would give the appropriate energy matching and thus allow the study of the influence of the translational motion of the water proton nuclei on the cross-effect. Interestingly, the DNP enhancements of about -3 achieved for the bTbK are very similar to the enhancements obtained with monoradicals, e.g., TEMPO under identical experimental conditions (Fig. 7). This shows that for the Overhauser-driven DNP effect, only the mobility of the solvent or local motions of the N–O group, which are not affected by the overall size of the radical, are important. Additionally, the accessibility of the solvent protons to the unpaired spin seems to be very similar for the bTbK and TEMPO (see Ref. [20] for the review of the Overhauser DNP theory and experimental results in low magnetic fields).

5 Conclusions and Outlook

A rigid biradical (bTbK) with an optimized geometry for SS-DNP has been characterized by CW- and pulse-EPR experiments performed at X- and G-band frequencies. The coupling between the two unpaired electron spins is dipolar with a negligible exchange coupling. The two **g**-tensor axis systems are rotated approximately 90° around the x-axis with respect to each other. This geometry is optimal for efficient SS-DNP enhancements. Liquid-state DNP experiments performed at 260 GHz with the bTbK reveal purely Overhauser DNP enhancements, comparable in magnitude with results obtained for monoradicals [21, 22]. The main reason is the fast tumbling of the bTbK, leading to a motional narrowed EPR spectrum. To verify if the cross-effect can also be utilized in liquids to further increase the DNP enhancement, the biradical would have to be immobilized by enlarging its size or by rigidly binding to a large macromolecule. Work in this direction is under progress.

Acknowledgments We want to thank Burkhard Endeward for experimental support, Deniz Sezer, Mark Prandolini for many fruitful discussions and Dominik Margraf for comments on this paper. This project is funded by the European Commission in the design study project BIO-DNP.

References

1. K.M. Salikhov (ed.), Appl. Magn. Reson. **34**, 213–544 (2008)
2. A.V. Kessenikh, V.I. Lushchikov, A.A. Manenkov, Y.V. Taran, Sov. Phys. Solid State **5**, 321–329 (1963) [Fiz. Tverd. Tela **5**, 443–451 (1963)]
3. A. Abragam, W.G. Proctor, Compt. Rend. **246**, 2253–2256 (1958)
4. T. Maly, G. Debelouchina, V. Bajaj, K.-N. Hu, Ch.-G. Joo, M.L. Mak–Jurkauskas, J.R. Sirigiri, P. van der Wel, J. Herzfeld, R. Temkin, R.G. Griffin, J. Chem. Phys. **128**(052211), 1–19 (2008)
5. C. Song, K. Hu, C. Joo, T. Swager, R.G. Griffin, J. Am. Chem. Soc. **128**, 11385–11390 (2006)
6. K.-N. Hu, C. Song, H.-H. Yu, T.M. Swager, R.G. Griffin, J. Chem. Phys **128**(052302), 1–17 (2008)
7. V.N. Parmon, A.I. Kokorin, G.M. Zhidomirov, J. Struct. Chem. **18**, 104–147 (1977) [Zh. Strukt. Khim. **18**, 132–177 (1977)]
8. V.N. Parmon, A.I. Kokorin, G.M. Zhidomirov, J. Magn. Reson. **28**, 339–349 (1977)
9. Y. Matsuki, T. Maly, O. Ouari, H. Karoui, F. Le Moigne, E. Rizzato, S. Lyubenova, J. Herzfeld, T. Prisner, P. Tordo, R.G. Griffin, Angew. Chem. Int. Ed. 121, 5096–5100 (2009)
10. M.M. Hertel, V.P. Denysenkov, M. Bennati, T.F. Prisner, Magn. Reson. Chem **43**, S248–S255 (2005)
11. B. Epel, I. Gromov, S. Stoll, A. Schweiger, D. Goldfarb, Conc. Magn. Reson. **26B**, 36–45 (2005)
12. J. Low, Phys. Rev. **105**, 793–800 (1957)
13. O. Burghaus, M. Plato, M. Rohrer, K. Möbius, F. MacMillan, W. Lubitz, J. Phys. Chem. **97**, 7639–7647 (1993)
14. V.P. Denysenkov, M.J. Prandolini, A. Krahn, M. Gafurov, B. Endeward, T.F. Prisner, Appl. Magn. Reson. **34**, 289–299 (2008)
15. S. Stoll, A. Schweiger, J. Magn. Reson. **178**, 42–55 (2006)
16. D. Margraf, B.E. Bode, A. Marko, O. Schiemann, T.F. Prisner, Mol. Phys. **105**, 2153–2160 (2007)
17. M.A. Ondar, A.A. Dubinskii, O.Ya. Grinberg, I.A. Grigor'ev, L.B. Volodarskii, Ya.S. Lebedev, J. Struct. Chem. **22**, 525–531 (1981) [Zh. Strukt. Khim. **22**, 59–66 (1981)]
18. V.I. Gulin, S.A. Dikanov, Yu.D. Tsvetkov, Chem. Phys. Lett. **170**, 211–216 (1990)
19. A.W. Overhauser, Phys. Rev. **92**, 411–415 (1953)
20. J. Potenza, Adv. Mol. Relax. Proc. **4**, 229–354 (1972)
21. M.J. Prandolini, V.P. Denysenkov, M. Gafurov, B. Endeward, T.F. Prisner, J. Am. Chem. Soc. **131**, 6090–6092 (2009)
22. M.J. Prandolini, V. Denysenkov, M. Gafurov, S. Lyubenova, B. Endeward, M. Bennati, T. Prisner, Appl. Magn. Reson. **34**, 399–407 (2008)